NASA/TP-20210020403

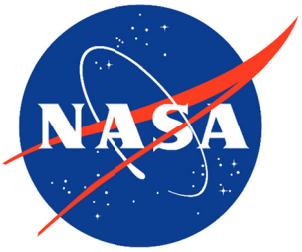

Neutron Diffusion Correction in 3DHZETRN-V2: ENDF/B

John W. Wilson
Old Dominion University Research Foundation, Norfolk, Virginia

Tony C. Slaba, Charles M. Werneth
Langley Research Center, Hampton, Virginia

Francis F. Badavi
Old Dominion University Research Foundation, Norfolk, Virginia

Brandon D. Reddell
Johnson Space Center, Houston, Texas

Amir A. Bahadori
Kansas State University, Manhattan, Kansas

August 2021

The NASA STI Program Office . . . in Profile

Since its founding, NASA has been dedicated to the advancement of aeronautics and space science. The NASA Scientific and Technical Information (STI) Program Office plays a key part in helping NASA maintain this important role.

The NASA STI Program Office is operated by Langley Research Center, the lead center for NASA's scientific and technical information. The NASA STI Program Office provides access to the NASA STI Database, the largest collection of aeronautical and space science STI in the world. The Program Office is also NASA's institutional mechanism for disseminating the results of its research and development activities. These results are published by NASA in the NASA STI Report Series, which includes the following report types:

- TECHNICAL PUBLICATION. Reports of completed research or a major significant phase of research that present the results of NASA programs and include extensive data or theoretical analysis. Includes compilations of significant scientific and technical data and information deemed to be of continuing reference value. NASA counterpart of peer-reviewed formal professional papers, but having less stringent limitations on manuscript length and extent of graphic presentations.

- TECHNICAL MEMORANDUM. Scientific and technical findings that are preliminary or of specialized interest, e.g., quick release reports, working papers, and bibliographies that contain minimal annotation. Does not contain extensive analysis.

- CONTRACTOR REPORT. Scientific and technical findings by NASA-sponsored contractors and grantees.

- CONFERENCE PUBLICATION. Collected papers from scientific and technical conferences, symposia, seminars, or other meetings sponsored or co-sponsored by NASA.

- SPECIAL PUBLICATION. Scientific, technical, or historical information from NASA programs, projects, and missions, often concerned with subjects having substantial public interest.

- TECHNICAL TRANSLATION. English-language translations of foreign scientific and technical material pertinent to NASA's mission.

Specialized services that complement the STI Program Office's diverse offerings include creating custom thesauri, building customized databases, organizing and publishing research results ... even providing videos.

For more information about the NASA STI Program Office, see the following:

- Access the NASA STI Program Home Page at ***http://www.sti.nasa.gov***

- E-mail your question via the Internet to help@sti.nasa.gov

- Fax your question to the NASA STI Help Desk at (301) 621-0134

- Phone the NASA STI Help Desk at (301) 621-0390

- Write to:
  NASA STI Help Desk
  NASA Center for AeroSpace Information
  7115 Standard Drive
  Hanover, MD 21076-1320

NASA/TP-20210020403

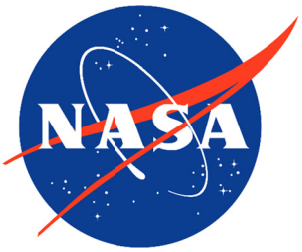

Neutron Diffusion Correction in 3DHZETRN-V2: ENDF/B

John W. Wilson
Old Dominion University Research Foundation, Norfolk, Virginia

Tony C. Slaba, Charles M. Werneth
Langley Research Center, Hampton, Virginia

Francis F. Badavi
Old Dominion University Research Foundation, Norfolk, Virginia

Brandon D. Reddell
Johnson Space Center, Houston, Texas

Amir A. Bahadori
Kansas State University, Manhattan, Kansas

National Aeronautics and
Space Administration

Langley Research Center
Hampton, Virginia 23681-2199

August 2021

Available from:

NASA Center for AeroSpace Information (CASI)
7115 Standard Drive
Hanover, MD 21076-1320
(301) 621-0390

National Technical Information Service (NTIS)
5285 Port Royal Road
Springfield, VA 22161-2171
(703) 605-6000

Contents

Figures

I. Abstract

A recent study of neutron leakage from a uniform cube of aluminum showed some hope of implementing a simple diffusion correction for the 3DHZETRN code in spite of an oversimplified neutron scattering dataset. Still, this transport of internally generated isotropic sources of neutrons resulted in improved but somewhat inaccurate estimates (±20 percent) of neutron leakage in non-hydrogenous materials. This especially occurs for neutrons produced by normal incident protons onto a laterally extended but relatively thin geometry, such as that encountered in space construction. In the present report, we discuss and improve on this simple approach to correct for this error, in addition to introducing an improved neutron scattering dataset (ENDF/B).

II. Introduction

We commissioned a study to better understand the effects of differing nuclear cross sections through a sensitivity analysis [Heinbockel et al. 2005, Wilson et al. 2005] and direct comparison [Wilson et al. 2005; Heinbockel et al. 2009, 2011a,b] with NASA related Monte Carlo (MC) codes (FLUKA and HETC). It was found that the solution is sensitive to errors in the few to several nucleon removal cross sections for heavy projectiles, and also errors in the production of neutrons and light ions. Recent 3DHZETRN code development [Wilson et al. 2014a-c, 2015] used a forward/isotropic representation of the neutron production and scattering cross sections, wherein the forward component is represented by a straight-ahead approximation with isotropic components treated as an angle dependent first order perturbation (similar to removal/diffusion theory [Wilson and Lamkin 1974]). The generated field equation for isotropic neutron sources was solved using a bi-directional (forward/backward) approximation over N ray directions, and provided a converging sequence of solutions for increasing number of rays as N =1, 2, 6, 10, etc.

This 3DHZETRN solution method agreed with individual MC codes Geant4 version 9.4.6 [Agostinelli et al. 2003; Geant4 2012a,b; Koi 2008], FLUKA [Battistoni et al. 2007, Aarnio et al. 1993, Andersen et al. 2004, Fasso et al. 2005] and PHITS version 2.64 [Niita et al. 2006; Sato et al. 2006, 2013; Sihver et al. 2007] to a greater degree than the MC codes agreed among themselves [Wilson et al. 2015]. This agreement occurred in spite of differing nuclear models/databases used in the four different codes [Slaba et al. 2017, Wilson et al. 2015, 2017a]. For example, see Fig. 1 comparing various implementations of the Serber [1947] model within MC codes to our recent Serber implementation [Wilson et al. 2020]. Advancement in the 3DHZETRN code depended less on improving numerical marching procedures and more on improvements to the nuclear database [Wilson et al. 2017a,b, 2020]. With recent improvements in the nuclear database [Wilson et al. 2020] we again turn attention to improved transport procedures.

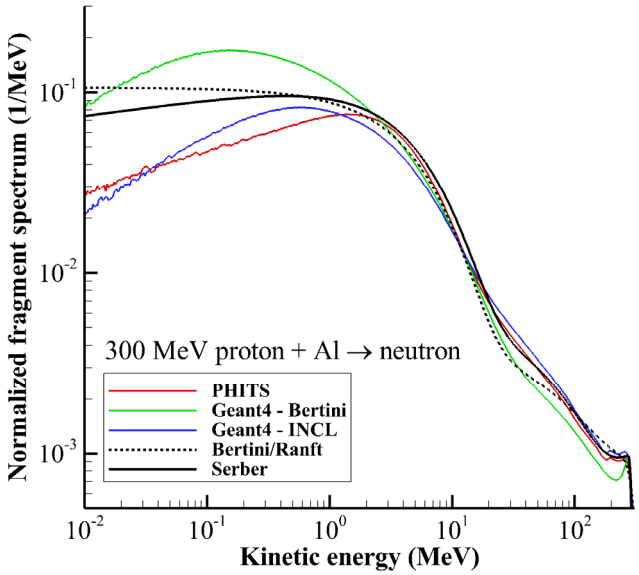

Fig. 1. Neutron production energy spectrum for 300 MeV protons incident on ^{27}Al. Results from implementations of the Serber model in MC simulation codes are compared to our recent work [Wilson et al. 2020].

In the recent past, we defined neutron leakage factors to isolate the transport properties of a material from the production properties allowing a better understanding of the effects of nuclear interaction differences among these codes [Wilson et al. 2015, 2017b, 2020; Slaba et al. 2017]. As a result of those studies, it was recognized that the bi-directional approximation to low-energy neutron transport underestimated the leakage near lateral boundaries. Although reasonable solutions are found for many materials and finite geometries, it was found that solutions along long rays nearly parallel to a near bounding surface overestimated the accumulated neutron fluence as a result of underestimating the leakage through the near boundary [Wilson et al. 2015].

In the present report, we will first re-examine the formalism and consider the impact of including a preliminary factor for diffusive losses of isotropic neutron sources within a material. The next section shows results of the simple diffusion correction compared to MC results. In the last section, we further look to a more complete representation of diffusive losses and improved neutron production using a recent Serber model [Wilson et al. 2020]. The more accurate ENDF/B [ENDF 2016] cross sections for neutron scattering are added as well.

III. Neutron Diffusion in 3DHZETRN-V2

The relevant transport equations are the coupled linear Boltzmann equations, derived on the basis of conservation principles [Wilson 1977, Wilson et al. 1991] for the differential flux (or fluence) density, $\phi_j(\mathbf{x},\mathbf{\Omega},E)$, of j-type particles in the continuous slowing down approximation, in which atomic/molecular processes are described by a stopping power, $S_j(E)$, [Wilson et al. 1991] for each ion type j (vanishes for neutrons) as

$$\mathbf{B}[\phi_j(\boldsymbol{x},\mathbf{\Omega},E)] = \sum_k \int_E^\infty \int_{4\pi} \sigma_{jk}(E,E',\mathbf{\Omega},\mathbf{\Omega}')\phi_k(\boldsymbol{x},\mathbf{\Omega}',E')\,d\mathbf{\Omega}'\,dE' - \sigma_j(E)\phi_j(\boldsymbol{x},\mathbf{\Omega},E)\,, \tag{1}$$

where $\mathbf{B}[\phi_j(\mathbf{x},\Omega,E)]$ is the Boltzmann operator describing drift in space and energy given as

$$\mathbf{B}[\phi_j(\boldsymbol{x},\mathbf{\Omega},E)] \equiv \mathbf{\Omega}\bullet\nabla\phi_j(\boldsymbol{x},\mathbf{\Omega},E) - \frac{1}{A_j}\frac{\partial}{\partial E}\big[S_j(E)\phi_j(\boldsymbol{x},\mathbf{\Omega},E)\big]\,, \tag{2}$$

and E is kinetic energy per amu. Equation (1) is to be solved subject to a boundary condition over the enclosure of the solution domain. At the present level of development, the double differential interaction cross sections, $\sigma_{jk}(\mathbf{\Omega},\mathbf{\Omega}',E,E')$, are represented by a forward directed quasi-elastic (*qe*) component, an angle dependent multiple-production (*mp*) component [Wilson et al. 2020], plus other processes such as evaporative de-excitation (*ev*) of the target nuclei, and elastic scattering of neutrons (*el*) represented by

$$\begin{aligned}\sigma_{jk}(E,E',\mathbf{\Omega},\mathbf{\Omega}') = \sigma_{k,abs}(E')\big\{F_{jk,qe}(E,E')\delta(\mathbf{\Omega}-\mathbf{\Omega}') + F_{jk,mp}(E,E')g_R(\theta,E,A_T)\big\}\\ +\tfrac{1}{4\pi}\sigma_{jk,ev}(E,E') + \delta_{nk}\sigma_{jk,el}(E,E',\mathbf{\Omega},\mathbf{\Omega}')\,.\end{aligned} \tag{3}$$

The first term of equation (3) represents the quasi-elastic multiple-scattered component with spectrum $F_{jk,qe}(E,E')$ assumed to travel straight forward. The second term is for those nucleons and other light ions resulting from intra-nuclear collisions of the quasi-elastic scattered primary particles with the target nuclear material, and are associated with broadly dispersed lower-energy particles [Ranft 1980] produced with energy distribution $F_{jk,mp}(E,E')$. At each energy, the angular dispersion of this term is taken from the Ranft angular factor used in early versions of FLUKA as is appropriate for sequences of two-body scatterings within nuclei [Ranft 1980],

$$g_R(\theta,E,A_T) = \begin{cases} N_R\exp(-\theta^2\,/\,\lambda_R) & ,\ 0\le\theta\le\pi\,/\,2 \\ N_R\exp(-\pi^2\,/\,4\lambda_R) & ,\ \pi\,/\,2<\theta\le\pi \end{cases}\,. \tag{4}$$

In equation (4), the production angle is $\theta = \cos^{-1}(\mathbf{\Omega}\bullet\mathbf{\Omega}')$, N_R is an energy dependent normalization factor, A_T is the target nuclear mass number, and the Ranft width factor is

$$\lambda_R = (0.12 + 0.00036A_T)\,/\,E\,. \tag{5}$$

Note that the normalization is $\int g_R(\theta,E,A_T)d\Omega = 1$. The third term of equation (3) includes isotropic produced fragments from target de-excitation processes, and the fourth term describes neutron elastic scattering as presently represented by Chew's impulse approximation [Chew 1951] plus a phenomenological *S*-wave (matching the neutron KERMA [Wilson et al. 1991]). The charged ion nuclear interactions are dominated by the stopping power at energies less than 20 MeV/amu as shown in Fig. 2 [Wilson et al. 2005]. At higher energies, the elastic scattering is dominated by forward scattering at small angles [Wilson et al. 1991] for which the charged projectile energy and direction is largely unchanged and is therefore ignored. Elastic scattering is treated only for neutrons, and the charged particle recoils are included.

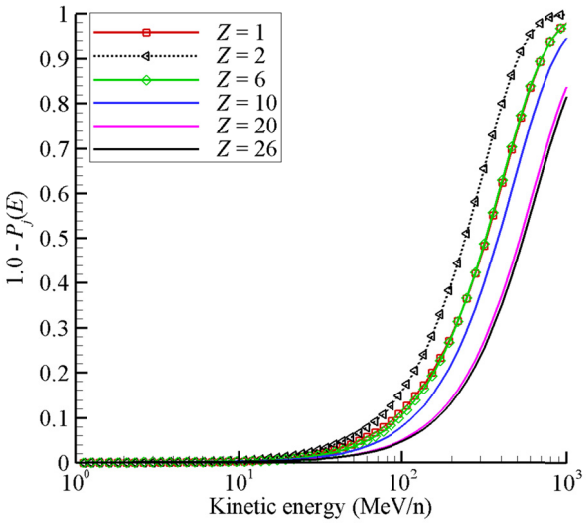

Fig. 2. Probability of nuclear interaction of ions with charge Z and energy MeV/n in coming to rest in aluminum.

In recent work, we replaced the Bertini/Ranft quasi-elastic term with results from an intra-nuclear transport Serber model yielding improved results [Wilson et al. 1986, 2015, 2017b, 2020]. The nucleonic quasi-elastic differential spectrum is found from

$$F_{jk,qe}(E,E') = f_{jk,qe}(E')\frac{2\pi\int \phi_{ms}[z(b),E,E']b\,db}{\pi R^2}\,, \tag{6}$$

where $z(b)$ is the target chord at impact parameter b, with $0 < b < R$, and R is the nuclear radius. The term $f_{jk,qe}(E')$ is the Bertini/Ranft branching ratio for multiple scattering [Wilson et al. 1988a,b, 1991, 2020], and $\phi_{ms}(z,E,E')$ is the spectrum of the multiple-scattered primary nucleon of initial energy E' after traveling a distance z in the target nuclear material found using intra-nuclear transport theory [Wilson et al. 1986, 2017b, 2020]. We further note that [Wilson et al. 2020]

$$\sigma_{jk,qe}(E,E',\mathbf{\Omega},\mathbf{\Omega}') \approx \sigma_{k,abs}(E')F_{jk,qe}(E,E')\delta(\mathbf{\Omega}-\mathbf{\Omega}')\,, \tag{7}$$

where $\sigma_{k,abs}(E')$ is take from quantum scattering theory [Wilson 1974, Wilson and Costner 1975].

The second term of equation (3) is for multiple-production (*mp*) representing highly spectrally dispersed particles of lower energy [Wilson 1977, Wilson et al. 1986] with energy spectral components as given in the current version of 3DHZETRN-v2.1 [Wilson et al. 2020] by

$$F_{jk,mp}(E,E') = f_{jk,mp}(E')\frac{2\pi\int \phi_{mr}[z(b),E,E']b\,db}{\pi R^2}\,, \tag{8}$$

where $f_{jk,mp}(E')$ is the Bertini/Ranft branching ratio for multiple production [Wilson et al. 1988a,b, 2017a, 2020], and $\phi_{mr}(z,E,E')$ is the main multiple recoil solution for a primary nucleon of initial energy E' from intra-nuclear transport theory [Wilson et al. 1986, 2017b, 2020]. We further note

$$\sigma_{jk,mp}(E,E',\mathbf{\Omega},\mathbf{\Omega}') \approx \sigma_{k,abs}(E')F_{jk,mp}(E,E')g_R(\theta,E,A_T)\,. \tag{9}$$

The target evaporative de-excitation spectrum is given by equation (10), where N_{jk} is the evaporation multiplicity with parameters from the Bertini model [Wilson et al. 1988a, 1991],

$$\sigma_{jk,ev}(E,E',\mathbf{\Omega},\mathbf{\Omega}') = \sigma_{k,abs}(E')N_{jk}\,\frac{\left(\frac{E}{\lambda}\right)^p e^{-\frac{E}{\lambda}}}{4\pi\gamma\left(1+p,\frac{E'}{\lambda}\right)}\ , \tag{10}$$

where $p = 0.1$, $\gamma(1+p,E'/\lambda)$ is the incomplete gamma function of the first kind, and λ is related to the average energy, $\langle E\rangle$, of produced particles according to

$$\left\langle E\right\rangle = \alpha\frac{\gamma\left(2+p,\frac{E'}{\lambda}\right)}{\gamma\left(1+p,\frac{E'}{\lambda}\right)}. \tag{11}$$

The average energies are given in Wilson et al. [1991, p. 212]. It is noted that the dependence of equation (11) on E' is weak, allowing quick convergence of the solution for λ, and in the limit that $E'/\lambda \gg 1$ is given as

$$\lambda \approx \left\langle E\right\rangle\frac{\Gamma(1+p)}{\Gamma(2+p)}\,. \tag{12}$$

with $\Gamma(p)$ being the (complete) gamma function. Note, the result of equation (12) can be used in an iterative sense in equation (11) for a more accurate evaluation of λ as

$$\alpha \approx \left\langle E\right\rangle\frac{\gamma\left(1+p,\frac{E'}{\lambda_0}\right)}{\gamma\left(2+p,\frac{E'}{\lambda_0}\right)}, \tag{13}$$

where λ_0 is the initial estimate given by equation (12).

The cross sections for elastic scattering of neutrons from target nuclei are discussed on pages 151, 152, and 367 of Wilson et al. [1991]. Within the straight-ahead version of HZETRN we have used the differential energy cross section as given by equation (4.96) in Wilson et al. [1991]. In a prior paper [Clowdsley et al. 2000, 2001], the elastic scattering was separated into forward ($\theta_L < \pi/2$) and backward hemispheres ($\theta_L > \pi/2$) with respect to the lab scattering angle $\theta_L = \cos^{-1}(\mathbf{\Omega}\bullet\mathbf{\Omega}')$. This provided an initial refinement of the straight-ahead approximation with some success [Heinbockel et al. 2011a,b; Slaba et al. 2020], and it should be noted the bi-directional approximation is a first correction to the traditional straight-ahead approximation that we have used in HZETRN for many years [Wilson and Lamkin 1975, Wilson et al. 1988c].

Within the bi-directional formalism, the neutron elastic cross section is written as

$$\sigma_{nn,el}(E,E',\mathbf{\Omega},\mathbf{\Omega}') = \tfrac{1}{4\pi}\Big[\sigma^{(f)}_{nn,el}(E,E') + \sigma^{(b)}_{nn,el}(E,E')\Big], \tag{14}$$

where the forward (f) and backward (b) elastic cross sections can be written as

$$\sigma^{(f)}_{nn,el}(E,E') = \Theta(\tfrac{\pi}{2}-\theta_L)\sigma_{nn,el}(E,E')\ , \tag{15}$$

$$\sigma^{(b)}_{nn,el}(E,E') = \Theta(\theta_L - \tfrac{\pi}{2})\sigma_{nn,el}(E,E')\,, \tag{16}$$

and $\Theta(x)$ is the unit step function. In equations (15) and (16), we have used the kinematic relationship between E, E', and θ_L, given by

$$E = E'\frac{A_T^2 + 2A_T\cos\left\{\theta_L + \sin^{-1}\left[\sin\left(\frac{\theta_L}{A_T}\right)\right]\right\} + 1}{(A_T+1)^2}\,. \tag{17}$$

In the present paper, we will further approximate the neutron elastic scattering into forward and isotropic terms, consistent with the model of Wilson et al. [2014a-c] previously applied for inelastic neutron production. This serves a next order correction to the bi-directional approximation. We now discuss the extension and integration of equations (14) - (17) into the forward/isotropic model.

The double differential cross sections within the transport formalism are approximated by a forward quasi-elastic component in equation (7), an anisotropic multiple-production component in equations (4) and (9), an isotropic target decay component in equation (10), and an angle dependent neutron elastic-scattering component (Chew impulse term [Chew, 1951] plus an *S*-wave) in equations (14) - (17). We further approximate the multiple production cross section as a forward (*for*) plus isotropic (*iso*) term given as

$$\sigma_{jk,mp}(E,E',\boldsymbol{\Omega},\boldsymbol{\Omega}') \approx \sigma^{(for)}_{jk,mp}(E,E',\boldsymbol{\Omega},\boldsymbol{\Omega}') + \tfrac{1}{4\pi}\sigma^{(iso)}_{jk,mp}(E,E')\,, \tag{18}$$

where the *mp* isotropic term is evaluated by integrating the double differential cross section over the backward hemisphere ($2\pi B$) according to

$$\sigma^{(iso)}_{jk,mp}(E,E') = 2\int_{2\pi B}\sigma_{jk,mp}(E,E',\boldsymbol{\Omega},\boldsymbol{\Omega}')\,d\boldsymbol{\Omega}\,. \tag{19}$$

The forward *mp* term is found by integrating over the forward hemisphere ($2\pi F$), yielding

$$\begin{aligned}\sigma^{(for)}_{jk,mp}(E,E') &= \int_{2\pi F}\left[\sigma_{jk,mp}(E,E',\boldsymbol{\Omega},\boldsymbol{\Omega}') - \tfrac{1}{4\pi}\sigma^{(iso)}_{jk,mp}(E,E')\right]d\boldsymbol{\Omega} \\ &= \sigma_{k,abs}(E')F_{jk,mp}(E,E')\int_0^{\pi/2} g_R(\theta,E,A_T)d\theta - \tfrac{1}{2}\sigma^{(iso)}_{jk,mp}(E,E')\end{aligned}\,. \tag{20}$$

With the demonstrated success of the bi-directional (forward/backward) approximation [Clowdsley et al. 2000, 2001, Wilson et al. 2005, Heinbockel et al. 2011a], the solution is similarly divided into forward and isotropic related components where the isotropic terms are treated as a first perturbation. The first order forward term, $\phi^{(for)}_j(\boldsymbol{x},\boldsymbol{\Omega},E)$, is defined to satisfy

$$\mathbf{B}[\phi^{(for)}_j(\boldsymbol{x},\boldsymbol{\Omega},E)] = \sum_k\int_E^\infty \sigma^{(for)}_{jk}(E,E')\phi^{(for)}_k(\boldsymbol{x},\boldsymbol{\Omega}',E')\,d\boldsymbol{\Omega}'\,dE' - \sigma_j(E)\phi^{(for)}_j(\boldsymbol{x},\boldsymbol{\Omega},E)\,, \tag{21}$$

where

$$\sigma^{(for)}_{jk}(E,E') = \sigma_{k,abs}(E')F_{jk,qe}(E,E') + \sigma^{(for)}_{jk,mp}(E,E') + \tfrac{1}{4\pi}\delta_{nk}f^{(for)}_{el}(E')\sigma_{nn,el}(E,E')\,. \tag{22}$$

The isotropic, $f^{(iso)}_{el}(E')$, and forward, $f^{(for)}_{el}(E')$, fractional contributions to elastic scattering are given in Fig. 3 and calculated as

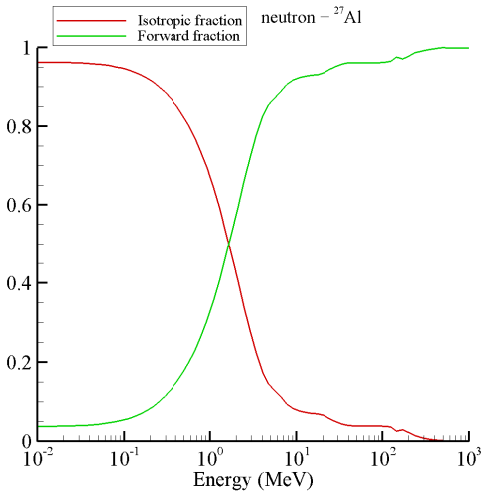

Fig. 3. Fractional contribution to elastic scattering by isotropic and forward scattered neutrons.

$$f_{el}^{(iso)}(E') = \frac{2}{\sigma_{n,el}(E')}\int_E \sigma_{nn,el}(E,E')dE\,, \tag{23}$$

$$f_{el}^{(for)}(E') = 1 - f_{el}^{(iso)}(E')\,. \tag{24}$$

Only the forward propagating fluence, $\phi_j^{(for)}(\boldsymbol{x},\boldsymbol{\Omega},E)$, appears in the transport of equation (21) circumventing the need to evaluate an off-axis integral seen in equation (1). Note that $\boldsymbol{\Omega}$ enters into this equation as a parameter and can be evaluated according to the boundary condition that we set as the incident fluence from direction $\boldsymbol{\Omega}_0$ as shown in Fig. 4. The forward propagated fluence can be evaluated, subject to the boundary condition, at all locations within the interior of the prescribed geometry.

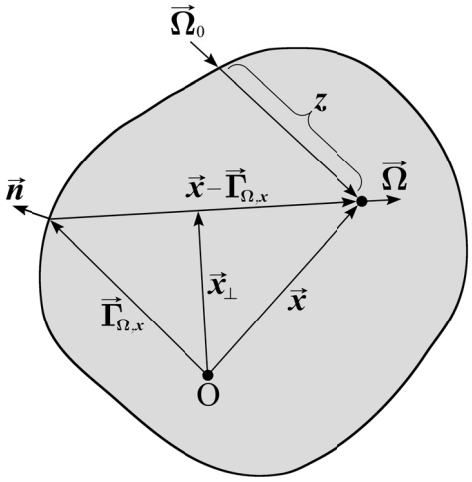

Fig. 4. Geometry of 3D marching procedure.

The full solution includes the perturbed (*prt*) field that is coupled to the forward solution through the cross section,

$$\sigma_{jk}^{(prt)}(E,E',\mathbf{\Omega},\mathbf{\Omega}') = \frac{1}{4\pi}\Big[\sigma_{jk,mp}^{(iso)}(E,E') + \sigma_{jk,ev}(E,E') + \delta_{nk} f_{el}^{(iso)}(E')\sigma_{nn,el}(E,E')\Big]. \tag{25}$$

The coupling between the forward field, $\phi_j^{(for)}(\boldsymbol{x},\mathbf{\Omega},E)$, and the isotropically produced particle field, $\phi_j^{(prt)}(\boldsymbol{x},\mathbf{\Omega},E)$, appears in the perturbing source term within the equation

$$\begin{aligned}\mathbf{B}[\phi_j^{(prt)}(\boldsymbol{x},\mathbf{\Omega},E)] = &\sum_k \int_E^\infty \int_{4\pi} \sigma_{jk}(E,E',\mathbf{\Omega},\mathbf{\Omega}')\phi_k^{(prt)}(\boldsymbol{x},\mathbf{\Omega}',E')\,d\mathbf{\Omega}'\,dE' - \sigma_j(E)\phi_j^{(prt)}(\boldsymbol{x},\mathbf{\Omega},E) \\ &+\sum_k \int_E^\infty \sigma_{jk}^{(prt)}(E,E',\mathbf{\Omega},\mathbf{\Omega}_0)\phi_k^{(for)}(\boldsymbol{x},\mathbf{\Omega}_0,E')\,dE' \ .\end{aligned} \tag{26}$$

Once the unperturbed forward fluence, $\phi_j^{(for)}(\boldsymbol{x},\mathbf{\Omega},E)$, is evaluated using equations (21) and (22) for direction $\mathbf{\Omega}_0$ over the domain of $\boldsymbol{x}$ and E, one must yet solve for the perturbed fluence, $\phi_j^{(prt)}(\boldsymbol{x},\mathbf{\Omega},E)$, within the target configuration given in equation (26) that again involves the troublesome integral over $d\Omega'$. Note that the last term in equation (26) contains the perturbing isotropic source of particles from collisions of the forward propagating fluence given as

$$\xi_j^{(prt)}(\boldsymbol{x},\mathbf{\Omega},\mathbf{\Omega}_0,E) = \sum_k \int_E^\infty \sigma_{jk}^{(prt)}(E,E',\mathbf{\Omega},\mathbf{\Omega}_0)\phi_k^{(for)}(\boldsymbol{x},\mathbf{\Omega}_0,E')\,dE', \tag{27}$$

for which the forward fluence, $\phi_j^{(for)}(\boldsymbol{x},\mathbf{\Omega},E)$, is a function of the penetration depth z along the direction $\mathbf{\Omega}_0$. We denote this by replacing $\xi_j^{(prt)}(\boldsymbol{x},\mathbf{\Omega},\mathbf{\Omega}_0,E)$ with $\chi_j^{(prt)}[z(\boldsymbol{x}),\mathbf{\Omega},\mathbf{\Omega}_0,E]$ where $z(\boldsymbol{x})$ is the penetration depth along $\mathbf{\Omega}_0$ to the point $\boldsymbol{x}$. Equation (26) is then rewritten as

$$\begin{aligned}\mathbf{B}[\phi_j^{(prt)}(\boldsymbol{x},\mathbf{\Omega},E)] = &\sum_k \int_E^\infty \int_{4\pi} \sigma_{jk}(E,E',\mathbf{\Omega},\mathbf{\Omega}')\phi_k^{(prt)}(\boldsymbol{x},\mathbf{\Omega}',E')\,d\mathbf{\Omega}'\,dE' - \sigma_j(E)\phi_j^{(prt)}(\boldsymbol{x},\mathbf{\Omega},E) \\ &+\chi_j^{(prt)}[z(\boldsymbol{x}),\mathbf{\Omega},\mathbf{\Omega}_0,E] \ .\end{aligned} \tag{28}$$

Note that equations (27) and (28) also provide a basis for introducing anisotropic source terms as we will do in a later section [Wilson et al. 2017a,b, 2020]. Whereas the forward propagating solution has its source fixed by the boundary condition, the perturbation solution (having no inbound fluence) is driven by internal (perturbing) sources generated by the collisions of the forward propagating inbound fluence, as modified by the forward propagator in penetrating to $\boldsymbol{x}$ along direction $\mathbf{\Omega}_0$. Solving equation (28) is hindered by the angular dependence of the scattering term, $\sigma_{jk}(\mathbf{\Omega},\mathbf{\Omega}',E,E')$, as were the original total field equations (1) and (3) above, and has been alleviated in the past by using the forward/backward approximation with some success [Clowdsley et al. 2000, 2001, Wilson et al. 2014b] that we will now employ to approximately solve the perturbation equation (28).

To solve the first order perturbation of equation (28), one must know the fluence, $\phi_j^{(prt)}(\boldsymbol{x},\mathbf{\Omega},E)$, at every $\boldsymbol{x}$ from all directions $\mathbf{\Omega}'$ approaching $\boldsymbol{x}$ from adjacent locations. This perturbed fluence is not known *a priori*. Developing an algorithm to approximately solve the perturbed fluence equation (28) is expedited by separating the perturbed fluence into forward and backward propagating components (a bi-directional approximation as we had used for many years [Clowdsley et al. 2000, 2001]) at a given direction $\mathbf{\Omega}$, and approximating the double differential cross sections as having forward/backward components [Wilson et al. 2017a] as

$$\sigma_{jk}(E,E',\mathbf{\Omega},\mathbf{\Omega}') \approx \sigma_{jk}^{(f)}(E,E')\delta(\mathbf{\Omega}-\mathbf{\Omega}') + \sigma_{jk}^{(b)}(E,E')\delta(\mathbf{\Omega}+\mathbf{\Omega}') \ , \tag{29}$$

where $\sigma_{jk}^{(f)}(E,E')$ is obtained by integrating the full double differential cross section over the forward hemisphere relative to $\mathbf{\Omega}$, and $\sigma_{jk}^{(b)}(E,E')$ is obtained by integrating over the corresponding backward hemisphere. Again we have assumed that the interaction cross sections can be separated in current usage by a product of angular dependent factors and an energy dependent factor as discussed above. It is clear that $\mathbf{\Omega}$ enters equation (28) as a parameter and can be solved along any arbitrary number of directions (rays), allowing construction of a numerical representation of $\phi_j^{(prt)}(\boldsymbol{x},\mathbf{\Omega},E)$ whose $\mathbf{\Omega}$ dependence, in part, comes from distance to the boundary, $t(\Omega)$ and $-t(-\Omega)$, with the penetration depth z along $\mathbf{\Omega}_0$.

The isotropic perturbation source in equation (28) effectively decouples the incident direction $\mathbf{\Omega}_0$ from the direction of propagation along $\mathbf{\Omega}$. The use of the bi-directional approximation in solving equation (28) is based on the assumption that losses along the ray $\mathbf{\Omega}$ are compensated by lateral diffusion from adjacent rays [Wilson et al. 2014a]. This is especially important for neutrons (and other neutral particles) with minimal atomic interactions allowing extensive drift. It is a demonstrated useful assumption in infinite media [Wilson et al. 2014a,b], but the approximation leads to overestimated fluence in any finite object. In this later case, it is only those rays within the subtended angle of the source, $\Delta\Omega$, as seen from the target point that mainly contribute. The remaining rays outside this $\Delta\Omega$ are directed towards the bounding surface of the solution domain and do not contribute to the first order perturbation solution at $\boldsymbol{x}$ (but rather leak through the boundary). In the present preliminary evaluation, the subtended angle is written as a fraction of the hemisphere $F(R,\delta_0) \le 1$ as

$$\Delta\Omega(R,\delta_0) = 2\pi F(R,\delta_0) \approx \frac{\pi\delta_0^2}{2R^2}, \tag{30}$$

where R is the distance along $\mathbf{\Omega}$ from the target point to the source at $\boldsymbol{x}$, and δ_0 is the minimum distance of the source point to the bounding surface in the plane perpendicular to $\mathbf{\Omega}$ at $\boldsymbol{x}$. The forward and backward cross sectional components for the drifting neutrons are evaluated within this solid angle as

$$\begin{aligned}\sigma_{nk}^{(f)}(E,E') &= \int_{\Delta\Omega(R,\delta_0)} \sigma_{nk}(E,E',\mathbf{\Omega},\mathbf{\Omega}')\,d\mathbf{\Omega} \\ &= \sigma_{k,abs}(E')F_{nk,qe}(E,E') + \sigma_{nk,mp}^{(for)}(E,E') + \tfrac{1}{4\pi}\delta_{nk}f_{el}^{(for)}(E')\sigma_{nn,el}(E,E') \\ &\quad +\Delta\Omega(R,\delta_0)\Big[\sigma_{nk,mp}^{(iso)}(E,E') + \sigma_{nk,ev}(E,E') + \tfrac{1}{4\pi}\delta_{nk}f_{el}^{(iso)}(E')\sigma_{nn,el}(E,E')\Big],\end{aligned} \tag{31}$$

$$\begin{aligned}\sigma_{nk}^{(b)}(E,E') &= \int_{\Delta\Omega(R,\delta_0)} \sigma_{nk}(E,E',-\mathbf{\Omega},\mathbf{\Omega}')\,d\mathbf{\Omega} \\ &= \Delta\Omega(R,\delta_0)\Big[\sigma_{nk,mp}^{(iso)}(E,E') + \sigma_{nk,ev}(E,E') + \tfrac{1}{4\pi}\delta_{nk}f_{el}^{(iso)}(E')\sigma_{nn,el}(E,E')\Big].\end{aligned} \tag{32}$$

In this, the straight forward produced neutrons add fully to the transport process, while the isotropically produced neutrons can exhibit significant leakage according to equations (31) and (32). Using equations (30) - (32) and the isotropic fraction for non-elastic cross sections in evaluation of equation (28) seems a reasonable approximation in most human rated vehicles, leading to an extension of transport of neutrons along an arbitrary ray $\mathbf{\Omega}$ as a solution to the bi-directional (forward/backward) equations [Clowdsley et al. 2000, 2001],

$$\begin{aligned}\mathbf{\Omega}\bullet\nabla\phi_n^{(prt)}(\boldsymbol{x},\mathbf{\Omega},E) &= \sum_k \int_E^\infty \sigma_{nk}^{(f)}(E,E')\phi_k^{(prt)}(\boldsymbol{x},\mathbf{\Omega},E')\,dE' \\ &\quad +\sum_k \int_E^\infty \sigma_{nk}^{(b)}(E,E')\phi_k^{(prt)}(\boldsymbol{x},-\mathbf{\Omega},E')\,dE' \\ &\quad -\sigma_n(E)\phi_n^{(prt)}(\boldsymbol{x},\mathbf{\Omega},E) + \chi_n^{(prt)}[z(\boldsymbol{x}),\mathbf{\Omega},\mathbf{\Omega}_0,E]\ ,\end{aligned} \tag{33}$$

$$-\boldsymbol{\Omega}\bullet\nabla\phi_n^{(prt)}(\boldsymbol{x},-\boldsymbol{\Omega},E)=\sum_k\int_E^\infty\sigma_{nk}^{(f)}(E,E')\phi_k^{(prt)}(\boldsymbol{x},-\boldsymbol{\Omega},E')\,dE'$$
$$+\sum_k\int_E^\infty\sigma_{nk}^{(b)}(E,E')\phi_k^{(prt)}(\boldsymbol{x},\boldsymbol{\Omega},E')\,dE' \tag{34}$$
$$-\sigma_n(E)\phi_n^{(prt)}(\boldsymbol{x},-\boldsymbol{\Omega},E)+\chi_n^{(prt)}[z(\boldsymbol{x}),-\boldsymbol{\Omega},\boldsymbol{\Omega}_0,E]\ .$$

Equation (34) for the backward moving field was obtained by replacing $\boldsymbol{\Omega}$ with $-\boldsymbol{\Omega}$ in equation (33). Equations (33) and (34) are solved simultaneously for no additional external fluence incident on the media boundary directed along $\boldsymbol{\Omega}$ (see Fig. 4). Note that the implicit assumption of equations (33) and (34) is that lateral diffusion from a given ray $\boldsymbol{\Omega}$ is compensated by diffusion from available adjacent rays. This has been demonstrated as a reasonable assumption for semi-infinite slab geometry [Heinbockel et al. 2011a,b; Wilson et al. 2014a,b,c]. The lateral leakage along $\boldsymbol{\Omega}_0$ in this case is found to a first order approximation by solving equations (33) and (34) along each $\boldsymbol{\Omega}_i$ between the ray limits $\{-t(-\boldsymbol{\Omega}_i),\ t(\boldsymbol{\Omega}_i)\}$ for a given set of $i = 1$ to N directions, $\boldsymbol{\Omega}_i$. The second order and higher order leakage is a consequence of solving equations (33) and (34) with the anti-leakage factor, $\Delta\Omega(R,\delta_0)$, of equations (31) and (32).

IV. Evaluation of Initial Model

Simple geometry and source orientation are chosen to allow efficient MC simulation for comparison with the calculation of quantities with the above formalism. In this way, the solution methodology is verified and experience is gained in the formalism, in preparation for connecting to the general geometric descriptions generated by the engineering design processes for which MC simulation remains impractical. Still, the MC methods play an important role in testing the development of highly efficient computational procedures as has been demonstrated, and utilized over nearly five decades of development [Wilson and Lamkin 1974, Wilson et al. 1991, 2005, 2014a,b,c, 2015, 2017a,b, 2020].

To test these ideas, we consider a 40 g/cm^2 (thick) homogeneous slab of aluminum with sides extending to infinity. We also consider a subset of the slab (cube) as shown in Fig. 5. The transport within the slab has leakage from the cube subset as noted in the upper figure exactly compensated by lateral diffusion into the subset as shown. The Webber representation of the February 23, 1956 solar particle event (an exponential rigidity spectrum with p_0 = 100 MV and 10^9 protons/cm^2 above 30 MeV [Webber 1966]) is assumed incident from above to test lateral diffusion processes. It is clear from Wilson et al. [2015] that lateral leakage is minimal for the lateral extension of 500 g/cm^2 and larger. For comparison, we also show results from Geant4, PHITS, and FLUKA. Removing the 40 g/cm^2 cube from the slab, as shown in the lower half of Fig. 5, leaves the leakage from the cube that is no longer compensated by diffusion from the exterior slab into the cube. Note that the isotropic collisional perturbing source, $\xi_j^{(prt)}(\boldsymbol{x},\boldsymbol{\Omega},\boldsymbol{\Omega}_0,E)$, within the cube is the same while embedded within the slab as when exposed singularly.

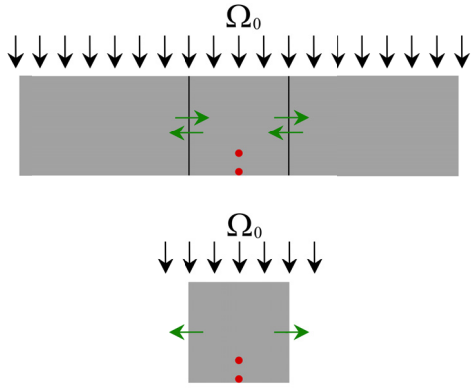

Fig. 5. Slab geometry and cube subset for present evaluation. Red circles indicate evaluation points (detectors). Green arrows indicate lateral leakage relationships between the geometries.

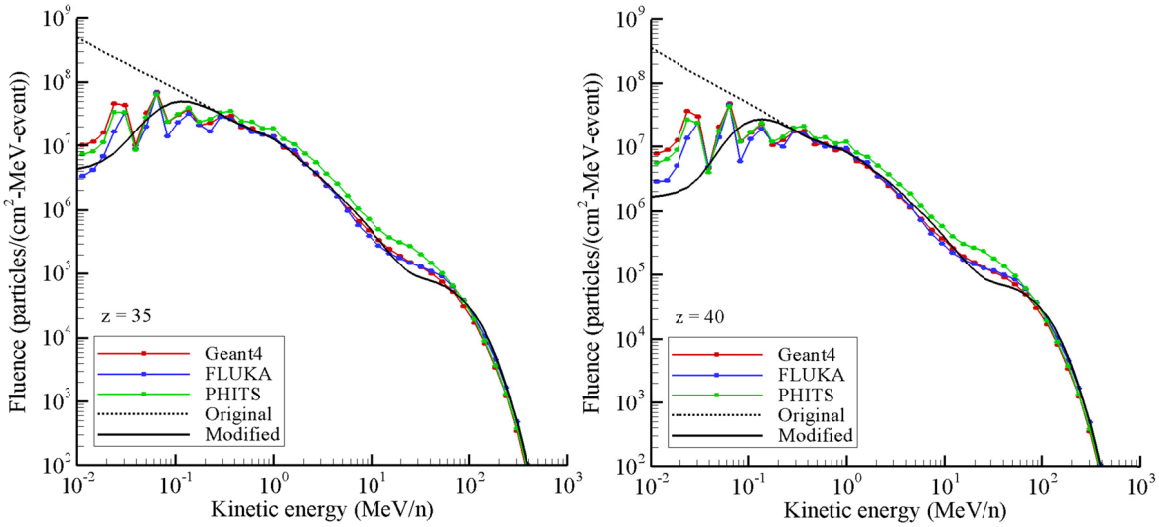

Fig. 6. Preliminary diffusion correction test for solution in slab geometry using the Bertini/Ranft model [Wilson et al. 2014a] at depths of 35 and 40 g/cm^2.

The solution with no leakage correction (i.e. $F(R,\delta) = 1$) at the two locations on the centerline of the cube (z = 35, 40 g/cm^2) is shown as the dashed curve in Fig. 6, with increases at the lowest energies (resulting from underestimating leakage) in comparison with results including the modifying factor in equation (30) and the result of MC simulations. At energies above 1 MeV, the present calculation is in reasonable agreement with the MC codes as seen in the figure. At the lower energies, where forward and absorptive processes for neutrons are minimal, the leakage through the slab faces along the long transport paths parallel or nearly parallel to the slab faces were underestimated in the prior formalism resulting in the increase of fluence on the centerline at these low energies (dashed curve) that is now approximately corrected in the present formalism. Clearly the improved propagation methods provided meaningful corrections for this problem as seen in Fig. 6. Encouraged by these results, we now seek refinements to the procedures of the above formalism.

Four limitations to be improved are first the perturbation is assumed isotropic, second the corresponding anisotropic portion is taken as being straight forward, third the elastic scattering cross sections are overly simple approximations, and fourth the subtended angle is underestimated by assuming that the distance to the boundary in all directions is the minimum distance as in equation (30). We now consider alternatives that reduce these limitations.

V. Refined Model

The fractional contribution of isotropic and forward elastic scattering are controlling factors and are shown for the current model as solid lines in Fig. 7. The low energy neutrons (the isotropic fraction) are expected to dominate leakage estimates. The isotropic fraction, as evaluated from the ENDF/B dataset, is also shown as dashed lines in Fig. 7 compared to that of the current dataset that we have used for many years [Wilson et al. 1991], displayed in, and utilized in the results of Fig. 6.

With the promising results in Fig. 6 for neutron production terms, we now seek improvements in the angular description of the elastic scattering and multiple-production terms, and to add a more detailed representation of the subtended angle of the perturbing source. We first improve the angular dependence within the transport formalism by limiting the contributions to the forward cross section to the quasi-elastic and forward elastic scattering events as

$$\sigma_{jk}^{(for)}(E,E') = \sigma_{k,abs}(E')F_{jk,qe}(E,E') + \tfrac{1}{4\pi}\delta_{nk}f_{el}^{(for)}(E')\sigma_{nn,el}(E,E'). \qquad (35)$$

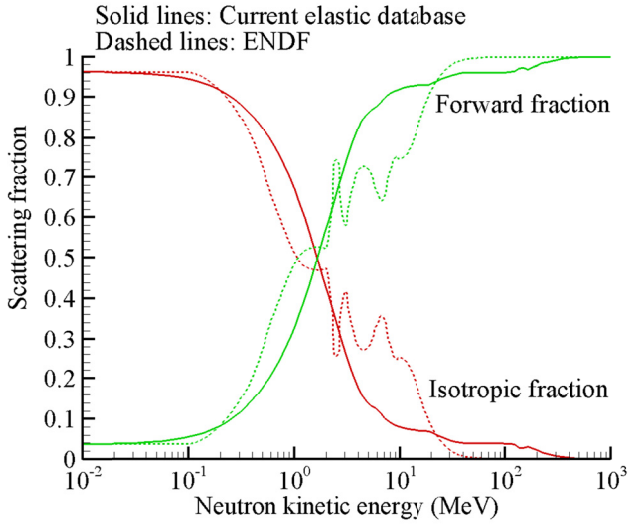

Fig. 7. Fractional contribution to elastic scattering by isotropic and forward scattered neutrons.

The multiple-production (*mp*) cross section no longer appears as a straight forward component. It will instead enter as an angle dependent perturbation along with target decay products and isotropic elastic scattering. The forward fluence, $\phi_j^{(for)}(\boldsymbol{x},\boldsymbol{\Omega},E)$, is again evaluated from equation (21) but using the more restricted cross section in equation (35). The cross section used to evaluate the angular dependent perturbing source of particles is now given by

$$\sigma_{jk}^{(prt)}(E,E',\boldsymbol{\Omega},\boldsymbol{\Omega}') = \sigma_{jk,mp}(E,E',\boldsymbol{\Omega},\boldsymbol{\Omega}') + \frac{1}{4\pi}\Big[\sigma_{jk,ev}(E,E') + \delta_{nk} f_{el}^{(iso)}(E')\sigma_{nn,el}(E,E')\Big]. \tag{36}$$

The first order fluence perturbation, $\phi_j^{(prt)}(\boldsymbol{x},\boldsymbol{\Omega},E)$, is again found by solving equation (28), but with the angular dependent cross section in equation (36). Note that the perturbing source, $\chi_j^{(prt)}[z(\boldsymbol{x}),\boldsymbol{\Omega},\boldsymbol{\Omega}_0,E]$, is to be solved over the ray collection $\boldsymbol{\Omega}_i$ capturing the full impact of the correct geometry in this first order term, and hence, the first order effects of leakage are evaluated in solving equation (28) over the rays. The bi-directional propagator evaluates higher order leakage within the integration of $\sigma_{jk}(\boldsymbol{\Omega},\boldsymbol{\Omega}',E,E')$ over the corresponding forward and backward hemispheres that must be accounted.

In section IV, it was the modifications of the isotropic re-scattering that was modified by leakage that resulted in these higher order leakage corrections. The subtended angle of these higher order sources, as estimated in section IV, was based on the minimum distance of the source point to the boundary. This is a clear overestimate of the higher order leakage since each direction from the source point to the boundary on the plane perpendicular to $\boldsymbol{\Omega}$ is greater than or equal to the minimum. We will now treat the subtended angle in M sectors around the source point. Each sector has a distance of the source point to the boundary, δ_m, for which the effective subtended angle is

$$\Delta\Omega(R,\delta_m) = 2\pi F(R,\delta_m) \approx \frac{\pi\delta_m^2}{2MR^2}, \tag{37}$$

and the total subtended angle is the sum over all sectors as

$$\Delta\Omega = 2\pi\sum_{m=1}^{M} F(R,\delta_m). \tag{38}$$

The forward and backward produced cross sectional components for neutrons are found by replacing $\Delta\Omega(R,\delta_0)$ in equations (31) to (34) by $\Delta\Omega$ of equation (38).

VI. Evaluation of Refined Model

The calculated fluence using the new method for leakage correction (equations (37) and (38)) within the 40 g/cm^2 slab at 35 and 40 g/cm^2 depths are shown in Fig. 8 in comparison with the three MC codes (FLUKA, Geant4, PHITS) and various versions of 3DHZETRN. All the codes use differing nuclear databases (see Appendix A of Wilson et al. [2014a,b, 2020]) that accounts for some of the differences in Fig. 8 (also compare Fig. 1). The curve labeled "original" is that obtained using the Bertini/Ranft cross sections without corrections for diffusive losses. The "modified" curve has the diffusion factor of equation (38) accounting for losses in the Serber formalism replacing the Bertini/Ranft functions. In addition to replacing the Bertini/Ranft cross sections, the "modified (ENDF)" has the neutron elastic scattering of the Chew plus *S*-wave replaced by the ENDF/B neutron scattering data set. In the slab geometry being compared in Fig. 8, the neutron leakage only occurs through the front and back faces of the slab. The current treatment of diffusive losses in this case appears reasonable.

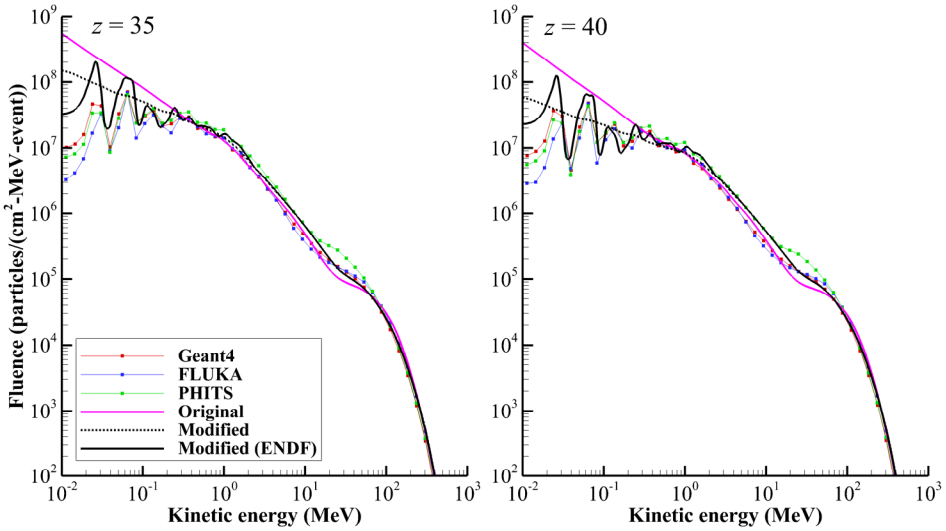

Fig. 8. Neutron fluence induced by the Webber SPE event [Webber 1966] in a 40 g/cm^2 slab of aluminum.

As a further test of this version of code, we compare the computational procedures where lateral leakage plays a role in cube geometry as shown in Fig. 9. Additional leakage is represented by comparing the results in the cube to that in spherical geometry (sphere with diameter specified to be the same as cube dimension in Fig. 5) given in Fig. 10. It is clear that the qualitative shifts due to increased leakage in the sphere is well represented by the modified versions and best represented by the ENDF version of the code.

While the current form of the diffusion correction is reasonably accurate there are still differences. It is clear that at this point of development, the current implementation is in greater agreement with the PHITS result as one might have guessed by the cross section differences in Fig. 1 and the fact that the same elastic scattering data set (ENDF/B) is used in all four codes. Still the ENDF/B implementation in 3DHZETRN2.1 has approximations noted in equation (14) - (16) that are not used in the MC codes. The elastic scattering is presently separated into two sectors (forward/backward) and the extension into six or more sectors may further improve the results.

VII. Conclusions

The focus of the present study was neutron production and propagation. The production has been improved by a fundamental quasi-elastic and multiple production model through the implementation of a semi-classical Serber transport model in nuclear matter. The quasi-elastic process is represented in the transport by a straight-ahead approximation, while the multiple production is at broad angles distributed according to the Ranft angular factor. A neutron leakage model is implemented through an effective solid angle of the source plane as seen from the

evaluation point. Neutron sources outside this angle are assumed to leak through the material boundary of the shield object and be lost from further consideration. This simple rule was demonstrated using modern Monte Carlo codes in the same source geometry and mass distribution.

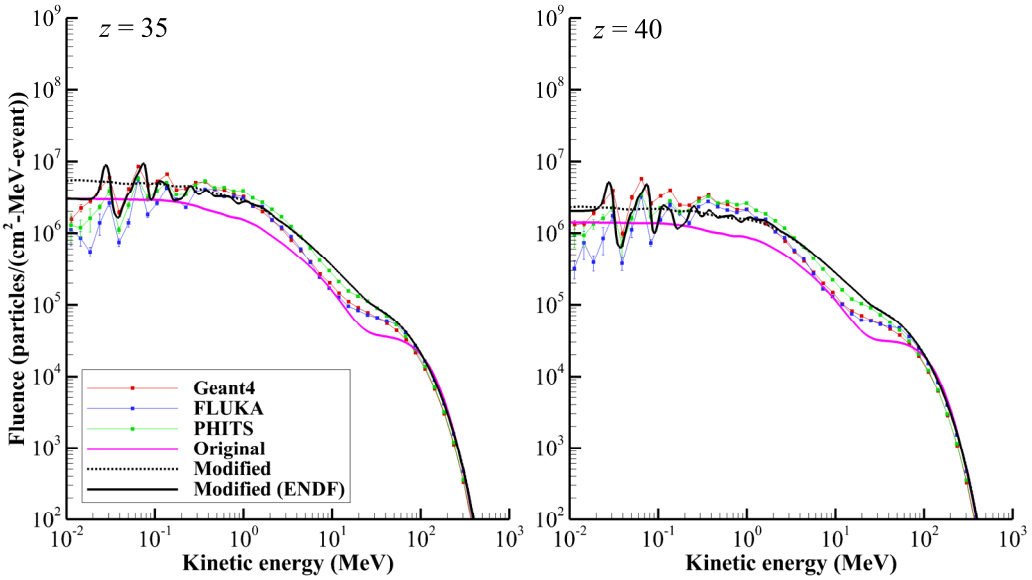

Fig. 9. Diffuse corrected fluence (modified) induced by the Webber SPE event [Webber 1966] in a 40 g/cm^2 aluminum cube at two depths according to the revised formalism. Also with ENDF/B elastic data set.

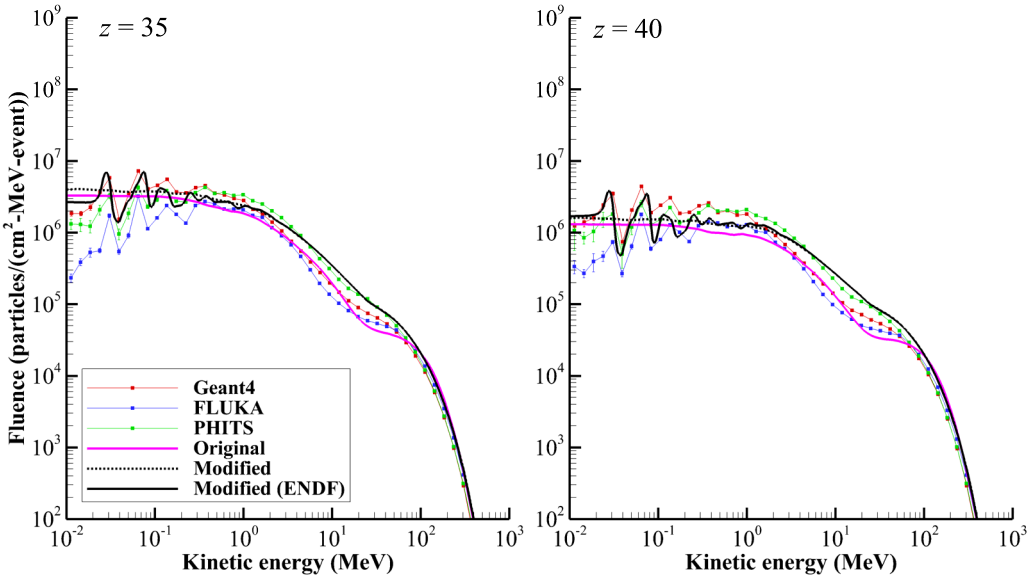

Fig. 10. Diffuse corrected fluence (modified) induced by the Webber SPE event [Webber 1966] in a 40 g/cm^2 aluminum sphere at two depths according to the revised formalism. Also with ENDF/B elastic data set.

VIII. Acknowledgements

This work was supported by the Advanced Exploration Systems Program and Human Research Program under the Human Exploration and Operations Mission Directorate of NASA and by NASA Grant number NNX14AL77A.

IX. References

Aarnio, P.A., Fasso, A. Ferrari, A., Moehring, H.J., Ranft, J., Sala, P.R., Stevenson, G.R., Zazula, J.M., FLUKA: Hadronic benchmarks and applications. Proceedings of the MC93 International Conference on Monte Carlo Simulation in High Energy and Nuclear Physics; 1993.

Agostinelli, S., et al., Geant4--a simulation toolkit. *Nucl. Instrum. & Methods A* **506**: 250-303; 2003.

Andersen, V., Ballarini, F., Battistoni, G., Campanella, M., Carboni, M., Cerutti, F., Empl, A., Fasso, A., Ferrari, A., Gadioli, E., Garzelli, M.V., Lee, K., Ottolenghi, A., Pelliccioni, M., Pinsky, L.S., Ranft, J., Roesler, S., Sala, P.R., Wilson, T.L., The FLUKA code for space applications: recent developments. *Adv. Space Res.* **34**: 1338–1346; 2004.

Battistoni, G., Muraro, S., Sala, P.R., Cerutti, F., Ferrari, A., Roesler, S.,Fasso, A., Ranft, J., The FLUKA code: description and benchmarking. Proceedings of the Hadronic Shower Simulation Workshop 2006, **896**: 31–49; 2007.

Chew, G.F., High energy elastic proton-deuteron scattering. *Phys. Rev.* **84**: 1057-1058; 1951.

Clowdsley, M.S., et al. A comparison of the multigroup and collocation methods for solving the low-energy neutron Boltzmann equation. *Can. J. Phys*. **78**: 45-56; 2000.

Clowdsley, M.S., Wilson, J.W., Shinn, J.L., Badavi, F.F., Heinbockel, J.H., Atwell, W., Neutron environment calculations for low Earth orbit. SAE 01ICES2327; 2001.

ENDF, Evaluated nuclear data file database; 2016. Available at https://www-nds.iaea.org/exfor/endf.htm.

Fasso, A., Ferrari, A., Ranft, J., Sala, P.R., FLUKA: A multi-particle transport code, CERN-2005-10, INFN/TC 05/11, SLAC-R-773; 2005.

Geant4 Reference Physics Lists. Website: http://www.geant4.org/geant4/support/ physicsLists/referencePL/referencePL.shtml; 2012a.

Geant4 Recommended Physics Lists. Website: http://www.geant4.org/geant4/ support/physicsLists/referencePL/useCases.shtml; 2012b.

Heinbockel, J.H., Wilson, J.W., Blattnig, S.R., Qualls, G.D., Badavi, F.F., Cucinotta, F.A., Cross section sensitivity and propagated errors in HZE exposures. NASA TP 2005-213945; 2005.

Heinbockel, J.H., Slaba, T.C., Blattnig, S.R., Tripathi, R.K., Townsend, L.W., Handler, T., Gabriel, T.A., Pinsky, L.S., Reddell, B., Clowdsley, M.S., Singleterry, R.C., Norbury, J.W., Comparison of radiation transport codes HZETRN, HETC and FLUKA using the 1956 Webber SPE spectrum. NASA TP 2009-215560; 2009.

Heinbockel, J.H., Slaba, T.C., Blattnig, S.R., Tripathi, R.K., Townsend, L.W., Handler, T., Gabriel, T.A., Pinsky, L.S., Reddell, B., Clowdsley, M.S., Singleterry, R.C., Norbury, J.W., Badavi, F.F., Aghara, S.K., Comparison of the transport codes HZETRN, HETC and FLUKA for a solar particle event. *Adv. Space Res.* **47**: 1079-1088; 2011a.

Heinbockel, J.H., Slaba, T.C., Tripathi, R.K., Blattnig, S.R., Norbury, J.W., Badavi, F.F., Townsend, L.W., Handler, T., Gabriel, T.A., Pinsky, L.S., Reddell, B., Aumann, A.R., Comparison of the transport codes HZETRN, HETC and FLUKA for galactic cosmic rays. *Adv. Space Res.* **47**:1089-1105; 2011b.

Koi, T., New native QMD code in Geant4. IEEE Nuclear Science Symposium Conference Record, 2008.

Niita, K., Sato, T., Iwase, H., Nose, H., Nakashima, H., Sihver, L., 2006 PHITS - A particle and heavy ion transport code system, *Rad. Meas.* **41**: 1080-1090; 2006.

Ranft, J., The FLUKA and KASPRO hadronic cascade codes. Computer Techniques in Radiation Transport and Dosimetry. Plenum Press; 1980.

Sato, T., Niita, K., Iwase, H., Nakashima, H., Yamaguchi, Y., Sihver, L., Applicability of particle and heavy ion transport code PHITS to the shielding design of spacecrafts. *Rad. Meas.* **41**: 1142-1146; 2006.

Sato, T., Niita, K., Matsuda, N., Hashimoto, S., Iwamoto, Y., Noda, S., Ogawa, T., Iwase, H.,Nakashima, H., Fukahori, T., Okumura, K., Kai, T., Chiba, S., Furuta T., Sihver, L., Particle and heavy ion transport code system PHITS, version 2.52, *J. Nucl. Sci. Technol.* **50**: 913-923; 2013.

Serber, R. Nuclear Reactions at High Energies. *Phys. Rev*. **72**: 1114-1115; 1947.

Sihver, L., Mancusi, D., Sato, T., Niita, K., Iwase, H., Iwamoto, Y., Matsuda, N., Nakashima, H., Sakamoto, Y., Recent developments and benchmarking of the PHITS Code. *Adv. Space Res.* **40**: 1320-1331; 2007.

Slaba, T.C., Bahadori, A.A., Reddell, B.D., Singleterry, R.C., Clowdsley, M.S., Blattnig, S.R., Optimal shielding thickness for galactic cosmic ray environments. *Life Sci. Space Res.* **12**: 1-12; 2017.

Slaba, T.C., Wilson, J.W., Werneth, C.M., Whitman, K., Updated Deterministic Radiation Transport for Future Deep Space Missions. *Life Sci. Space Res.* **27**: 6-18; 2020.

Webber, W.R., An Evaluation of solar-cosmic-ray events during solar minimum. D2-84274-1, Boeing Co. 1966.

Wilson, J.W., Lamkin, S.L., Perturbation approximation to charged particle transport. *Trans. Am. Soc*., **19**: 443; 1974.

Wilson, J.W., Multiple scattering of heavy ions, Glauber theory, and optical model. *Phys. Lett. B* **52**: 149-152; 1974.

Wilson, J. W., Costner, C., Nucleon and heavy ion total and absorption cross section for selected nuclei. NASA TN D-8107; 1975.

Wilson, J.W., Lamkin, S.L., Perturbation theory for charged-particle transport in one dimension. *Nucl. Sci. & Eng.* **57**: 292-299; 1975.

Wilson, J.W., Analysis of the theory of high-energy ion transport. NASA TN D-8381, 1977.

Wilson, J.W., Townsend, L.W., Cucinotta, F.A., Transport model of nucleon-nucleus reaction. NASA TM 87724; 1986.

Wilson, J.W., Townsend, L.W., Chun, S.Y., Buck, W.W., Khan, F., Cucinotta, F.A., BRYNTRN: a baryon transport computer code computational procedures and data base. NASA TM-4037, 1988a.

Wilson, J.W., Chun, S.Y., Buck, W.W., Townsend, L.W., High energy nucleon data bases. *Health Phys*. **55**: 817-819; 1988b.

Wilson, J.W., Townsend, L.W., Ganapol, B. Chun, S.Y. Buck, W.W., Charged-particle transport in one dimension. *Nuc. Sci. Eng.* **99**: 285-287; 1988c.

Wilson, J.W., Townsend, L.W., Schimmerling, W., Khandelwal, G.S., Khan, F., Nealy, J.E., Cucinotta, F.A., Simonsen, L.C., Shinn, J.L., Norbury, J.W., Transport Methods and Interactions for Space Radiations. NASA RP-1257, 1991.

Wilson, J.W., Tripathi, R.K., Mertens, C.J., Blattnig, S.R., Clowdsley, M.S., Verification and validation: high charge and energy (HZE) transport codes and future development. NASA TP 2005-213784; 2005.

Wilson, J.W., Slaba, T.C., Badavi, F.F., Reddell, B.D., Bahadori, A.A., A 3DHZETRN code in a uniform sphere with Monte Carlo verification. NASA TP 2014-218271; 2014a.

Wilson, J.W., Slaba, T.C., Badavi, F.F., Reddell, B.B., Bahadori, A.A., Advances in NASA radiation transport research: 3DHZETRN. *Life Sci. Space Res.* **2**: 6-22; 2014b.

Wilson, J.W., Slaba, T.C., Badavi, F.F., Reddell, B.D., Bahadori, A.A., 3D space radiation transport in a shielded ICRU tissue sphere. NASA TP 2014-218530; 2014c.

Wilson, J.W., Slaba, T.C., Badavi, F.F., Reddell, B.D., Bahadori, A.A., 3DHZETRN: neutron leakage in finite objects. *Life Sci. Space Res.* **7**: 27-38; 2015.

Wilson, J.W., Werneth, C.M., Slaba, T.C., Badavi, F.F., Reddell, B.D., Bahadori, A.A., Neutron angular scatter effects in 3DHZETRN: quasi-elastic. NASA TP 2017-219597; 2017a.

Wilson, J.W., Slaba, T.C., Werneth, C.M., Badavi, F.F., Reddell, B.D., Bahadori, A.A., Advances in NASA radiation transport: 3DHZETRN-v2. NASA TP 2017-219665; 2017b.

Wilson, J.W., Werneth, C.M., Slaba, T.C., Badavi, F.F., Reddell, B.D., Bahadori, A.A., Effects of the Serber first step in 3DHZETRN-v2.1. *Life Sci. Space Res.* **26**: 10–27; 2020.

REPORT DOCUMENTATION PAGE

Form Approved
OMB No. 0704-0188

1. REPORT DATE *(DD-MM-YYYY)*	2. REPORT TYPE	3. DATES COVERED *(From - To)*
01/08/2021	Technical Publication	

4. TITLE AND SUBTITLE
Neutron Diffusion Correction in 3DHZETRN-V2: ENDF/B

5a. CONTRACT NUMBER

5b. GRANT NUMBER

5c. PROGRAM ELEMENT NUMBER

6. AUTHOR(S)
Wilson, John W.; Slaba, Tony C.; Werneth, Charles M.; Badavi, Francis F.; Reddell, Brandon D.; Bahadori, Amir A.

5d. PROJECT NUMBER

5e. TASK NUMBER

5f. WORK UNIT NUMBER
089407.01.23

7. PERFORMING ORGANIZATION NAME(S) AND ADDRESS(ES)
NASA Langley Research Center
Hampton, VA 23681-2199

8. PERFORMING ORGANIZATION REPORT NUMBER

9. SPONSORING/MONITORING AGENCY NAME(S) AND ADDRESS(ES)
National Aeronautics and Space Administration
Washington, DC 20546-001

10. SPONSOR/MONITOR'S ACRONYM(S)
NASA

11. SPONSOR/MONITOR'S REPORT NUMBER(S)
NASA-TP-20210020403

12. DISTRIBUTION/AVAILABILITY STATEMENT
Unclassified - Unlimited
Subject Category
Availability: NASA STI Program (757) 864-9658

13. SUPPLEMENTARY NOTES

14. ABSTRACT

A recent study of neutron leakage from a uniform cube of aluminum showed some hope of implementing a simple diffusion correction for the 3DHZETRN code in spite of an oversimplified neutron scattering dataset. Still, this transport of internally generated isotropic sources of neutrons resulted in improved but somewhat inaccurate estimates (±20 percent) of neutron leakage in non-hydrogenous materials. This especially occurs for neutrons produced by normal incident protons onto a laterally extended but relatively thin geometry, such as that encountered in space construction. In the present report, we discuss and improve on this simple approach to correct for this error, in addition to introducing an improved neutron scattering dataset (ENDF/B).

15. SUBJECT TERMS
space radiation; HZETRN; radiation transport

16. SECURITY CLASSIFICATION OF:			17. LIMITATION OF ABSTRACT	18. NUMBER OF PAGES	19a. NAME OF RESPONSIBLE PERSON
a. REPORT	b. ABSTRACT	c. THIS PAGE			HQ - STI-infodesk@mail.nasa.gov
U	U	U	UU	23	19b. TELEPHONE NUMBER *(Include area code)* 757-864-9658